Matthew J. Traum
Mem. ASME
Engineer Inc,
4832 NW 76th Rd,
Gainesville, FL 32653
e-mail: mtraum@alum.mit.edu

Fatemeh Hadi[1]
Mem. ASME
Mechanical and Manufacturing
Engineering Department,
Tennessee State University,
3500 John A. Merritt Blvd,
Nashville, TN 37209-1561
e-mail: fhadi@tnstate.edu

Muhammad K. Akbar
Mem. ASME
Mechanical and Manufacturing
Engineering Department,
Tennessee State University,
3500 John A. Merritt Blvd,
Nashville, TN 37209-1561
e-mail: makbar@tnstate.edu

Extending "Assessment of Tesla Turbine Performance" Model for Sensitivity-Focused Experimental Design

The analytical model of Carey is extended and clarified for modeling Tesla turbine performance. The extended model retains differentiability, making it useful for rapid evaluation of engineering design decisions. Several clarifications are provided including a quantitative limitation on the model's Reynolds number range; a derivation for output shaft torque and power that shows a match to the axial Euler Turbine Equation; eliminating the possibility of tangential disk velocity exceeding inlet working fluid velocity; and introducing a geometric nozzle height parameter. While nozzle geometry is limited to a slot providing identical flow velocity to each channel, variable nozzle height enables this velocity to be controlled by the turbine designer as the flow need not be choked. To illustrate the utility of this improvement, a numerical study of turbine performance with respect to variable nozzle height is provided. Since the extended model is differentiable, power sensitivity to design parameters can be quickly evaluated—a feature important when the main design goal is maximizing measurement sensitivity. The derivatives indicate two important results. First, the derivative of power with respect to Reynolds number for a turbine in the practical design range remains nearly constant over the whole laminar operating range. So, for a given working fluid mass flow rate, Tesla turbine power output is equally sensitive to variation in working fluid physical properties. Second, turbine power sensitivity increases as wetted disk area decreases; there is a design trade-off here between maximizing power output and maximizing power sensitivity.
[DOI: 10.1115/1.4037967]

Introduction

This paper extends the work of Carey and colleagues [1–3] to illustrate how Tesla turbine performance equations outlined therein inform practical design of a novel experimental turbine. A unique Tesla turbine was designed to experimentally measure the impact of a single design variable on power output. In turbine design, the goal is typically to maximize power generation, and it is therefore advantageous to select turbine parameters that maximize shaft power output. However, the purpose of this current work is to study how small parameter changes impact shaft power. Thus, the present study seeks to *maximize sensitivity of shaft power to a selected design variable*; mathematically, the magnitude of the partial derivate of shaft power with respect to the modulated variable. Thus, conventional Tesla turbine design approaches, which fix variables to maximize power output, have limited utility for the present experimental design. Instead, a differentiable closed-form analytical model relating geometric and working fluid parameters to Tesla turbine performance is needed.

The Tesla turbine was patented in 1913 [4]. Early attempts exist in the hobby literature to develop closed-form analytical solutions relating geometric and working fluid parameters to Tesla turbine performance [5,6]. The extensive Tesla turbine work of Rice and colleagues [7–11] and experiments of others [12–18] provide a rich foundation as do recent review articles [19,20]. A resurgent interest in Tesla turbines for their ability to process two-phase and particulate-laden working fluid characteristic of renewable energy systems (for example, working fluid of low thermodynamic quality from solar [21] or geothermal [22] sources as well as biomass combustion products [23]) has also motivated a number of theoretical studies and computational fluid dynamic modeling [24–29]. Other Tesla-type turbine research also exists. Barbarelli et al. [30], for example, posits a tangential flow turbine with a rotating channel containing five deflectors with possibility to achieve higher performance at low rotational velocity compared to conventional turbines. For other low-quality flows, such as low-head flows, use of a propeller pump instead of a conventional turbine is suggested [31]. However, the general focus of this whole body of Tesla turbine and related work is measuring and maximizing turbine power output.

While other closed-form analytical Tesla turbine models are available [32], we feel the work by Carey [1] represents the most easily modified differentiable closed-form analytical model relating geometric and working fluid parameters to Tesla turbine performance. It is therefore extended, utilized, and evaluated in this work, and the resulting new findings are reported.

Background

Carey's derivation begins with the Navier–Stokes equations in cylindrical coordinates applied to the rotating disk of a Tesla turbine [1,2]. It results in the following form for $\widehat{W}(\xi, \mathrm{Re}_m^*)$, the dimensionless tangential velocity difference between the disk rotor and fluid inside the turbine at any radial location

$$\widehat{W}(\xi) = \frac{e^{\frac{24\xi^2}{\mathrm{Re}_m^*}}}{\xi}\left[\frac{\mathrm{Re}_m^*}{24}e^{\frac{-24\xi^2}{\mathrm{Re}_m^*}} + \widehat{W}_o - \frac{\mathrm{Re}_m^*}{24}e^{\frac{-24}{\mathrm{Re}_m^*}}\right] \tag{1}$$

where $\xi = r/r_o$ is a dimensionless radial disk location; $\widehat{W}_o$ is the dimensionless relative disk/fluid velocity at the disk outer radius ($\xi = 1$); and Re_m^* is a modified Reynolds number

[1]Corresponding author.

Contributed by the Advanced Energy Systems Division of ASME for publication in the Journal of Energy Resources Technology. Manuscript received September 11, 2017; final manuscript received September 18, 2017; published online October 17, 2017. Editor: Hameed Metghalchi.

$$\mathrm{Re}_m^* = \frac{2b\dot{m}_c}{\pi\mu r_o^2} \tag{2}$$

The following turbine and working fluid parameters are then set: $\dot{m}_c$, ξ_i, b, ω, and $-v_{\theta,o}$, which facilitates solution for $\widehat{W}(\xi, \mathrm{Re}_m^*)$. Carey goes on to derive an expression for turbine efficiency

$$\eta = 1 - \frac{(\widehat{W}_i + \xi_i)\xi_i}{(\widehat{W}_o + 1)} \tag{3}$$

but an expression for turbine shaft power is not expressly given in Carey's paper [1].

Model Improvements

This work extends and clarifies the model of Carey [1], preserving its utility for Tesla turbine design by maintaining its differentiable closed-form analytical nature, by addressing the following five points:

- Identifying the model's Reynolds number limitation.
- Explaining how to obtain torque output by the turbine shaft.
- Developing an expression for Tesla turbine output shaft power.
- Introducing a simple nozzle geometric height parameter to obtain $-v_{\mathrm{nozzle}}$.
- Showing importance of checking maximum turbine rotational velocity.

Since these improvements preserve the differentiability and closed-form analytical nature of Eq. (3), efficiency (dimensionless power) can be differentiated with respect to ξ and Re_m^* to ascertain the sensitivity of turbine power output to each of these variable parameters. The location where the magnitude of $\partial\eta/\partial\xi$ is largest corresponds to the design point providing the highest sensitivity of power with respect to geometric disk parameters. The location where the magnitude of $\partial\eta/\partial\mathrm{Re}_m^*$ is largest corresponds to the design point providing the highest sensitivity of power with respect to working fluid thermodynamic properties. Maximum sensitivity locations in the design space correspond to dimensions and working fluid selections where a turbine should ideally be designed to provide the largest response to a changed experimental parameter to provide for more facile practical experimental measurement.

Model Reynolds Number Limitation. Two Reynolds numbers are presented in the Carey paper [1]. The first, Re_m^*, corresponds to Eq. (2) above, derived specifically for use in Eq. (1). The second, Re_m, is a more general Reynolds number based on mass flow rate and arising from nondimensionalization of the Navier–Stokes equations. This later more general Reynolds number is built up from the geometry for fluid flow between infinite flat plates. The two Reynolds numbers have the following relationship:

$$\frac{2b}{r_o}\mathrm{Re}_m = \mathrm{Re}_m^* \tag{4}$$

According to White, for the specific geometry of channels between flat plates, turbulent transition occurs at about $\mathrm{Re}_m \approx 2000$ [33]. Since the Carey model uses the laminar friction factor to quantify momentum transfer between the working fluid and disks, the effective valid Reynolds number range for model application is

$$0 < \mathrm{Re}_m = \frac{\dot{m}_c}{\pi\mu r_o} < 2000 \tag{5a}$$

$$0 < \mathrm{Re}_m^* = \frac{2b\dot{m}_c}{\pi\mu r_o^2} < \frac{2b\,2000}{r_o} \tag{5b}$$

where $\mathrm{Re}_m = \mathrm{Re}_m^* = 0$ represents no working fluid flow and mathematically causes Eq. (1) to return a null result.

Tesla Turbine Shaft Torque. Unlike internal combustion engines or conventional axial turbines, Tesla turbines typically deliver power at low torque and high rotational velocity, making it challenging to match their output to conventional generators or pumps [34,35]. Since rotational velocity is a set parameter in Carey's approach, generated torque is calculable from output shaft power

$$\Gamma = \frac{\dot{W}}{\omega} \tag{6}$$

Tesla Turbine Shaft Power. The conventional approach to derive turbine output shaft power for an axial turbine is application of the Euler Turbine Equation to working fluid inducing rotation of individual blades. However, in a Tesla turbine, the working fluid flows almost parallel to the disks instead of at near right angles. So, it is not intuitive that the Euler Turbine Equation can be applied.

Returning to steady-state Reynolds transport theorem for conservation of rotational momentum applied to working fluid interacting with a single disk yields the desired result. As shown in Fig. 1, a component of the working fluid, $-v_{\theta,i}$, exits tangent to the disk inner radius at all locations; although, the fluid flux at various locations may not be equal. This creates a boundary condition that appears complex to evaluate at firs. However, the integrated mathematical cross product in the Reynolds transport theorem resolves the complex condition into a vector of rotation about the turbine shaft

$$\sum \bar{\Gamma} = \int_{\mathrm{cs}} \rho[\bar{r} \times \bar{V}](\bar{V} \cdot \hat{n})dA \tag{7a}$$

$$\sum \bar{\Gamma} = \dot{m}\left([\bar{r} \times \bar{V}]_i - [\bar{r} \times \bar{V}]_o\right) \tag{7b}$$

Noting Eq. (6) and that the cross products in Eq. (7b) induce rotation about the turbine shaft, the vectors can be dropped to obtain

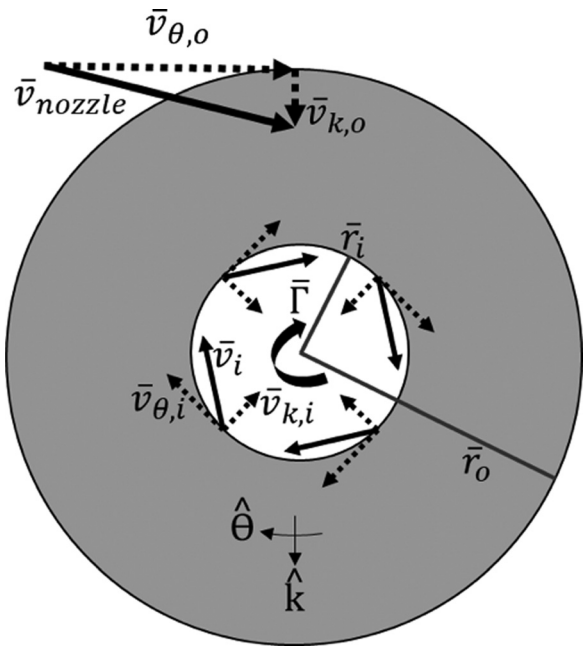

Fig. 1 Velocity vectors at the inlet and outlet of the Tesla turbine

$$\dot{W} = \omega\Gamma = \dot{m}\omega\left(v_{\theta,o}r_o - v_{\theta,i}r_i\right) \tag{8a}$$

$$\dot{W} = \dot{m}\left(v_{\theta,o}U_o - v_{\theta,i}U_i\right) \tag{8b}$$

Equation (8*b*) for a Tesla turbine does ultimately match the Euler turbine equation for an axial turbine. However, it was not intuitive without the derivation that the Tesla turbine and axial turbine expressions should match despite their differing geometries.

Nozzle Geometry Parameter to Obtain $\bar{v}_{\theta,o}$. In the model of Carey [1], $\dot{m}_c$, ξ_i, ω, and $\bar{v}_{\theta,o}$ are all user-defined parameters. If care is not exercised, the tangential velocity of the turbine disk at the inlet (set by ξ_i and ω) can exceed the tangential inlet working fluid velocity $\bar{v}_{\theta,o}$ and lead the model to return unphysical results. Also, careless combinations of $\dot{m}_c$ and $\bar{v}_{\theta,o}$ can imply need for nozzle throat areas on the scale of nanometers, which would be difficult to implement in practical fabrication.

Instead of setting $\dot{m}_c$ and $\bar{v}_{\theta,o}$, which can lead to both types of problems, it is recommend to set $\dot{m}$ and use a geometric nozzle parameter, h, to calculate $\bar{v}_{\text{nozzle}}$ and ultimately $\bar{v}_{\theta,o}$. As shown in Fig. 2, the nozzle orifice is treated as a rectangular slot with width defined by b, t, and n and height by h. With the inlet nozzle width fixed by choice of disk number, disk thickness, and disk spacing; nozzle inlet area is determined via a user-defined nozzle height parameter, h. This approach avoids erroneously selecting a nozzle velocity and mass flow rate requiring a nanometer diameter nozzle orifice. When designing a functioning Tesla turbine, $\dot{m}$ can be measured directly by determining the mass flow rate of working fluid available from the source (i.e., the compressor for a Brayton cycle turbine, the working fluid boiling rate for a Rankine cycle turbine, or the pump for a hydrodynamic turbine). From mass conservation, the resulting $\dot{m}_c$ and $\bar{v}_{\text{nozzle}}$ are

$$\dot{m}_c = \frac{\dot{m}}{n-1} \tag{9}$$

$$\bar{v}_{\text{nozzle}} = \frac{\dot{m}}{\rho h[nt + (n-1)b]} \tag{10}$$

where the working fluid density is a state property determined from the measured Tesla turbine nozzle pressure and temperature.

As seen in Fig. 1, $\bar{v}_{\text{nozzle}}$ can be trigonometrically deconstructed into two velocity vector components ($\bar{v}_{\theta,o}$ and $\bar{v}_{k,o}$) with respect to the polar coordinate reference frame of the disk. The tangential velocity component, $\bar{v}_{\theta,o}$, appears in Eqs. (8*a*) and (8*b*) imparting rotation to the turbine disks. The radial velocity component, $\bar{v}_{k,o}$, causes the fluid to move from the outer to the inner disk radius, inducing the Tesla turbine's characteristic spiral-shaped internal flow pattern. From mass continuity (Eq. (9) in Carey [1])

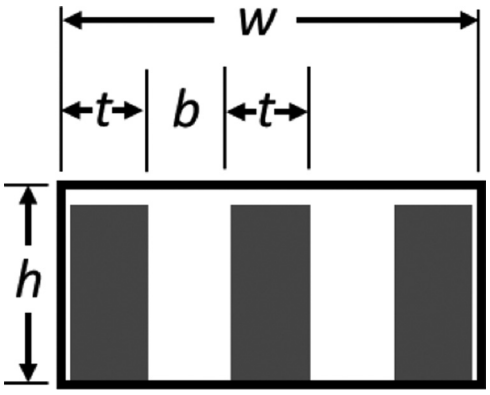

Fig. 2 Nozzle orifice schematic

$$\bar{v}_{k,r} = -\frac{\dot{m}_c}{2\pi r b \rho} \tag{11}$$

and from trigonometry

$$\bar{v}_{\theta,o} = \sqrt{\left(\bar{v}_{\text{nozzle}}\right)^2 - \left(\bar{v}_{k,o}\right)^2} \tag{12}$$

The denominator of Eq. (10) requires additional care because it yields $\bar{v}_{\text{nozzle}}$ corresponding to the nozzle throat flow velocity and not the flow velocity entering the interdisk channels, $\bar{v}_{\theta,\text{channel}}$. By continuity, the flow must speed up as it enters the interdisk channels since the disks create a barrier reducing the available flow area by $n \times h \times t$ below the nozzle throat area. Carey [1] clarifies that $\bar{v}_{\theta,o}$ is the intended velocity in the model, "… the tangential velocity at the rotor inlet is at or just above the [nozzle] throat sonic speed," which is confirmed by evaluating inlet conditions of the turbine evaluated in Carey. The speed of sound in steam at the modeled turbine inlet conditions (150 kPa and 436 K) is $c = 511.3$ m/s. Holding working fluid density constant to illustrate the case, Eqs. (10)–(12) together yield $\bar{v}_{\theta,o} = 478.04$ m/s (subsonic) while $\bar{v}_{\theta,\text{channel}} = 741.90$ m/s (supersonic). The fluid is able to accelerate into the interdisk turbine channels without actually crossing the sound barrier owing to the change in reference frame relative motion at the disk threshold. When the fluid is in the nozzle, the relative speed between the fluid and the nozzle arises from the fluid's velocity alone. By contrast, the linear speed of the disks is an appreciable fraction of the fluid's velocity. So, the fluid's reference frame changes as it passes into the inter disk channels from a fixed frame to a moving surrounding, resulting in a subsonic velocity relative to the tangential rotational velocity of the disks (741.90 m/s − 247.56 m/s = 494.35 m/s). The situation is similar to supersonic jets whose turbulent eddies are eliminated by enveloping the jet in co-flow that is both subsonic with respect to the central jet and to the quiescent surrounding air [36]. In a Tesla turbine, near-sonic flow from the nozzle can accelerate into the interdisk channels without violating continuity and without going supersonic because the relative velocity between the rotating disks and the flow is subsonic.

Availability of a nozzle geometric parameter, h, enables sensitivity of shaft power to be evaluated by mathematical derivative of power with respect to a nozzle dimension. Nozzle geometry is among the most important practical parameters influencing performance of Tesla turbines [1,2] as well as other turbomachinery devices [37], but nozzle geometry is absent in Carey's original model. With this modification, its influence can now be evaluated as part of a model that is a differentiable and closed-form analytical equation.

Maximum Turbine Rotational Velocity. Turbine rotational velocity, ω, remains a user-defined parameter in the revised model. However, $\bar{v}_{\theta,o}$ is now established based on the available measured working fluid mass flow rate and nozzle geometry instead of being arbitrarily set as in the Carey [1] model. In Carey, both mass flow rate and disk rotational velocity are free parameters, which creates the possibility of selecting a disk tangential velocity that exceeds the nozzle inlet velocity. There exists a practical upper bound on turbine rotational velocity because it is not physically possible for the disk tip speed to exceed working fluid flow velocity at the inlet [38,39]; this limit is enforced in the revised model

$$r_o\omega = U_o \leq \bar{v}_{\theta,o} \tag{13}$$

Results and Discussion

It is first shown that the extended model returns results in agreement with Carey's original. Second, the extended model's utility for design is illustrated by taking derivatives to determine sensitivity of efficiency (dimensionless power output) to selected variable parameters.

Table 1 Results of comparison between the original Tesla turbine analytical model [1] and the extended model of the present work

Variable	Units	Carey [1]	Extended model	% difference	Extended model—Carey#'s	% difference
P_{inlet}	(kPa)	150	150	0.0	150	0.0
T_{inlet}	(K)	436	436	0.0	436	0.0
μ_{water}	(kg/m-s)	1.34×10^{-5}	1.47×10^{-5}	10.5	1.34×10^{-5}	0.0
n	( )	18	18	0.0	18	0.0
ω	(rpm)	12,000	12,000	0.0	12,000	0.0
$\dot{m}$	(kg/s)	0.0421	0.0421	0.0	0.0421	0.0
b	(m)	0.001	0.001	0.0	0.001	0.0
r_o	(m)	0.197	0.197	0.0	0.197	0.0
r_i	(m)	0.0395	0.0395	0.0	0.0395	0.0
U_o	(m/s)	207	248	−19.6	207	0.0
$\tilde{W}_o$	( )	0.931	0.931	0.0	0.931	0.0
ξ	( )	0.2	0.2	0.0	0.2	0.0
Re_m	( )	281	272.21	3.1	298.62	−6.3
Re_m^*	( )	2.85	2.76	3.0	3.03	−6.4
$\tilde{W}_i$	( )	0.595	0.575	3.3	0.632	−6.2
η_m	( )	0.918	0.967	−5.4	0.951	−3.6

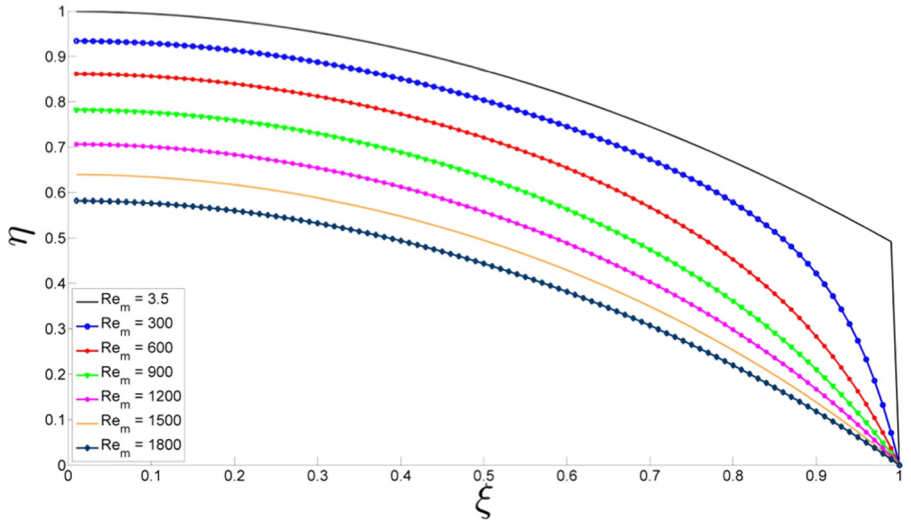

Fig. 3 Tesla turbine efficiency dependence on the ratio of rotor disk radii and Reynolds number. This result is consistent with plots in Carey [1].

Table 1 shows results from the extended model in comparison to the original model presented by Carey [1] for performance of a Tesla turbine in a solar-fired Rankine cycle using water as working fluid. The "STEAM_IAPWS" model in engineering equation solver was used to fix the working fluid inlet state ($P = 150$ kPa and $T = 436$ K) [40,41]. At this fixed thermodynamic state, Carey reports $\mu = 1.34 \times 10^{-5}$ kg/m-s; according to STEAM_IAPWS, the value should be $\mu = 1.47 \times 10^{-5}$ kg/m-s. Carey also reports $U_0 = 207$ m/s; however, calculating this value using Carey's method yields $U_0 = 248$ m/s. When corrected for the calculation inconsistencies, the extended model with Carey's numbers agrees with Carey's results within 6.4%.

As an additional comparison between Carey's work and the extended model, turbine efficiency (dimensionless power) is plotted in Fig. 3 as a function of ξ from $0 < \xi < 1$ over the laminar Reynolds number range, Eq. (5*a*), in increments of 300. The selected range of ξ encompasses disk geometries ranging from extremely radially thin disks with large central exit port ($\xi \approx 1$) to radially wide disks with small central exit port ($\xi \approx 0$). As expected, wider turbine disks ($\xi \to 0$) correspond to high power output because they present more surface area for momentum exchange with the working fluid and the fluid is in contact with the disk over a longer flow path before exiting the turbine. This outcome is identical to the results of Carey [1].

Turbine Performance: Varying Nozzle Height Versus Mass Flow Rate. Figure 4 illustrates the utility of adding a variable nozzle height parameter to the Tesla turbine model from both the perspective of a designer and an end user. In Carey's [1] original model, which assumed choked nozzle flow with no ability to modulate nozzle area, there is no way for a designer or end user to adjust turbine power output by changing working mass flow rate, $\dot{m}$. In the extended model where choked flow is not assumed, changing $\dot{m}$ simultaneously influences $\bar{v}_{k,r}$ [via Eq. (11)] and $\bar{v}_{\theta,o}$ [via Eqs. (10) and (12)], yielding an exponential fall-off in turbine efficiency with slight reduction in $\dot{m}$. By contrast, reducing the nozzle height, h, at fixed $\dot{m}$ induces a linear increase in turbine power output because only $\bar{v}_{\theta,o}$ is influenced with no change in $\bar{v}_{k,r}$. The flexibility created by adding a variable h to the model is interesting for multiple reasons. First, changing $\bar{v}_{\theta,o}$ at fixed $\bar{v}_{k,r}$ by varying h at fixed $\dot{m}$ influences the angle at which working fluid impinges on the turbine blades with velocity $\bar{v}_{\text{nozzle}}$ at the inlet, changing the shape of the spiraling fluid flow path between turbine blades. By adjusting h, a turbine designer can plan for and influence working fluid residence time inside the turbine, which can be important for minimizing disk damage owing to particulates in the flow or controlling heat transfer to the turbine housing. Second, it is known anecdotally that varying nozzle geometry is critical to optimizing Tesla turbine performance [42,43], and this

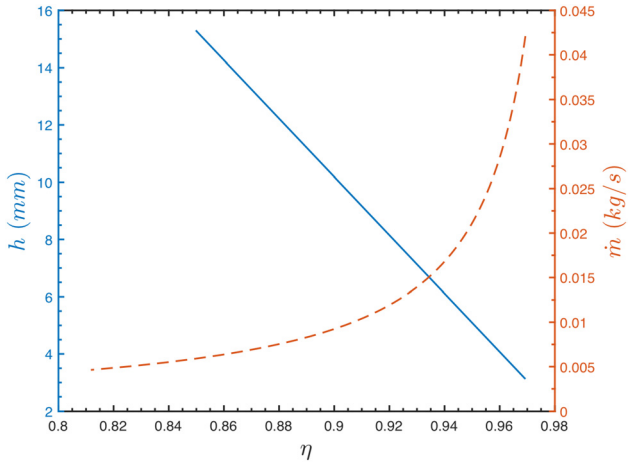

Fig. 4 Tesla turbine efficiency dependence on nozzle height, *h*, and mass flow rate, $\dot{m}$, differs due to the way these parameters impact $-v_{\theta,o}$ and $-v_{k,r}$

analysis reveals the reason. The linear change in turbine performance arising from adjusting h provides a more predictable and less fastidious means to optimize turbine performance than the nonlinear response induced by adjusting $\dot{m}$.

Derivatives to Assess Power Sensitivity for Design. The most important benefit of the extended Tesla turbine performance model for experimental design is the capability to evaluate its derivatives, $\partial\eta/\partial\xi$ and $\partial\eta/\partial\mathrm{Re}_m^*$. Their magnitude maxima within the viable ranges of ξ and Re_m^* indicate maximum sensitivity of power to variable experimental parameters influencing ξ and Re_m^*. The derivative $\partial\eta/\partial\xi$ is the following:

$$\frac{\partial\eta}{\partial\xi} = -\frac{\xi}{\widehat{W}_o + 1}\left[\frac{48}{\mathrm{Re}_m^*}\left(\widehat{W}_o - \frac{\mathrm{Re}_m^*}{24}\right)e^{\frac{24\left(\xi^2-1\right)}{\mathrm{Re}_m^*}} + 2\right] \tag{14}$$

Figure 5 shows $\partial\eta/\partial\xi$ as a function of ξ plotted for a range of Re_m^* values at increments of 300. The derivatives cluster for $0 < \xi \leq 0.5$ for all Reynolds numbers but begin to disperse over $0.5 < \xi \leq 0.85$ and achieve large relative magnitude beyond $0.85 < \xi$. However, this regime corresponds to low turbine blade wetted area and low power output with efficiencies below 60% for all Re_m (see Fig. 3, $\xi < 0.85$). In other words, disks with less wetted area provide greater experimental sensitivity. Typical turbine design emphasizes maximum power, i.e., Tesla turbines with large wetted disk area. There is therefore an engineering design trade-off here to be considered: decreasing disk wetted area to increase experimental sensitivity will simultaneously lower the turbine's total power output.

The derivative $\partial\eta/\partial\mathrm{Re}_m^*$ is the following:

$$\frac{\partial\eta}{\partial\mathrm{Re}_m^*} = -\frac{1}{\widehat{W}_o + 1}\left\{\frac{1}{24} - \left[\frac{24}{\mathrm{Re}_m^{*2}}\left(\widehat{W}_o - \frac{\mathrm{Re}_m^*}{24}\right)\left(\xi^2 - 1\right) + \frac{1}{24}\right]e^{\frac{24\left(\xi^2-1\right)}{\mathrm{Re}_m^*}}\right\} \tag{15}$$

Figure 6 shows $\partial\eta/\partial\mathrm{Re}_m$ as a function of Re_m plotted for a range of ξ values at increments of 0.1. For $\xi = 0.9$ and $\xi = 0.8$, the derivative magnitude is relatively large at low Reynolds number. The figure shows the derivative magnitude to be largest at $\xi = 0.9$ and $\mathrm{Re}_m \approx 200$. This locus of maximized sensitivity corresponds to low turbine power output and is not a practical design point. Moreover, for practical ξ values, such as for $\xi \leq 0.6$ (disks with relatively high wetted area), and especially over $500 < \mathrm{Re}_m < 2000$, the derivative is relatively flat, indicating little power sensitivity difference to Reynolds number across the laminar range. In short, Tesla turbine power output in the practical operating range is equally sensitive to changes in working fluid physical properties (i.e., density and viscosity) over the laminar Reynolds number range. From Fig. 6, Tesla turbine power output is almost insensitive to working fluid Reynolds number because the derivative in Eq. (15) is relatively small over the laminar Reynolds number operating range. Thus, for a given fixed turbine geometry and working fluid mass flow rate, variation in Tesla turbine power output is not significantly impacted by variation in working fluid Reynolds number in the laminar range. Because of the way Re_m^* influences Eq. (3) substantial differences in density or viscosity that change Reynolds number by more than three orders of magnitude at fixed turbine geometry (fixed ξ) induce a relatively small (less than one order of magnitude) change in efficiency (dimensionless power). For example, at $\xi = 0.2$, $\eta[\mathrm{Re}_m^* = 3.5] = 97.85\%$ while $\eta[\mathrm{Re}_m^* = 1800] = 56.01\%$ (see Fig. 3). This finding contrasts the observed and measured behavior of conventional small aero-derived turbines operating in the laminar range whose power output is highly sensitive to even slight changes in Reynolds number [44–46]. There is therefore another engineering trade-off here

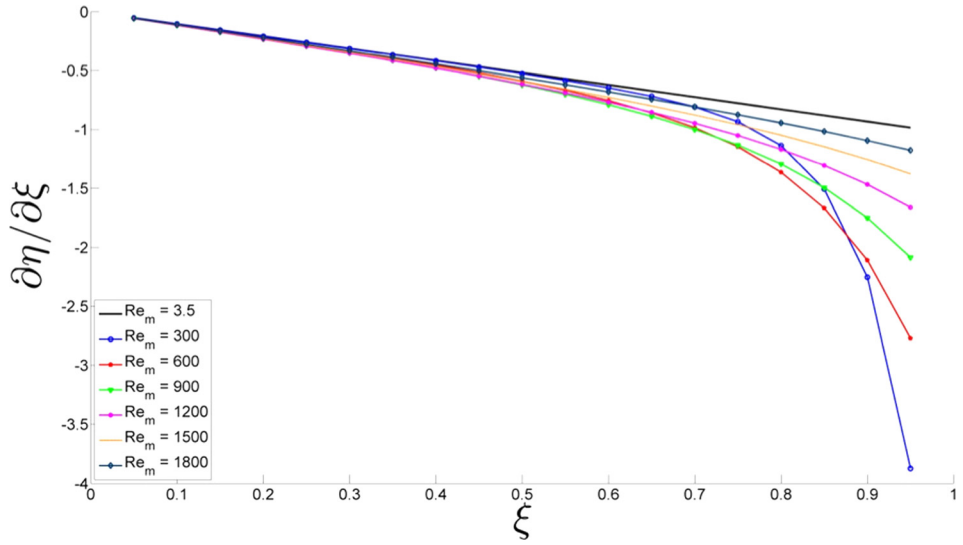

Fig. 5 The derivative of turbine efficiency (dimensionless power) with respect to ξ plotted for laminar Reynolds numbers

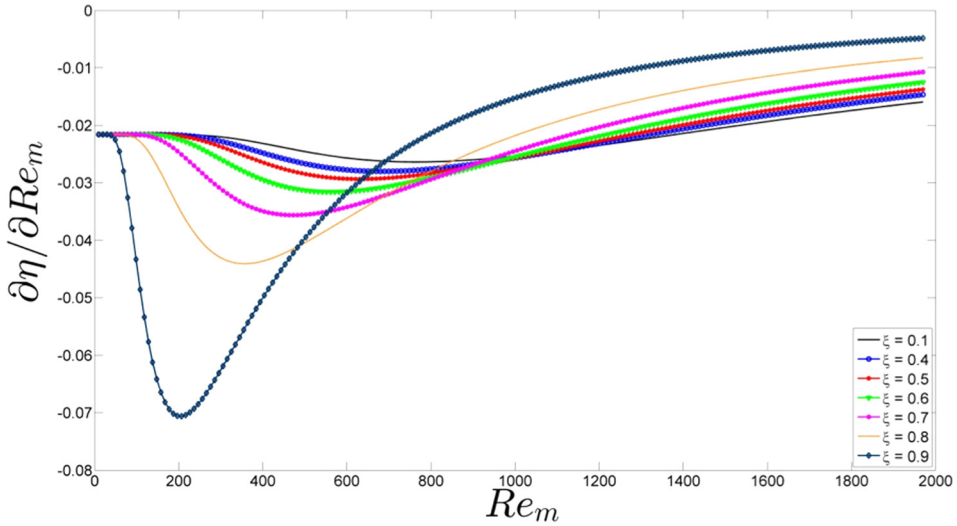

Fig. 6 The derivative of turbine efficiency (dimensionless power) with respect to Re_m plotted for $0.1 = \xi$ and $0.1 < \xi < 0.9$ at 0.1 increments

in working fluid selection. Fluids with high viscosity (low Re_m) drive up turbine efficiency. However, high viscosity fluids also incur higher parasitic energy losses than low viscosity fluids as they traverse the pipes and valves feeding the turbine. Figure 6 also informs another engineering benefit of Tesla turbines. Nearly constant Tesla turbine power sensitivity to Reynolds number for designs with wider turbine disks ($\xi \to 0$) and larger wetted areas also makes Tesla turbines attractive for power extraction scenarios where the viscosity or density (and hence Reynolds number) of working fluid changes intermittently and uncontrollably during operation; for example, in a terrestrial solar-fired power cycle or in space-based applications where the system is rapidly cycling between solar exposure and shade [47]. In the low sensitivity ($\xi \to 0$) design regime, Tesla turbine output power will change nominally and predictably despite large and uncontrolled changes in working fluid.

Conclusions

This work extends and clarifies the analytical model of Carey [1] to describe the performance of a Tesla turbine. The extended model retains the key feature of being a differentiable closed-form analytical equation to evaluate turbine shaft power output given user-determined geometric inputs of r_0, r_i, n, t, b, and h; working fluid parameters of $\dot{m}_c$, ρ, and μ; as well as the turbine rotational velocity, ω. A limitation on the model's viable Reynolds number range expressly stated, $0 < \mathrm{Re}_m = \dot{m}_c/\pi\mu r_o < 2000$. An expression for output shaft torque is also derived. The equation for Tesla turbine output shaft power is derived from first principles and shown to match the Euler Turbine Equation for power output of axial turbines. This outcome is not intuitive given differences between Tesla turbines and conventional axial turbines with respect to flow geometry and fluid–disk interaction. A check is introduced in the extended model to eliminate possibility that careless selected inputs could give tangential turbine disk velocity at the inlet exceeding tangential working fluid inlet velocity, which is physically impossible. A geometric nozzle parameter, h, is introduced to prevent selection of variables leading to a nozzle throat with unphysical dimensions on the order of nanometers or smaller. In addition, introduction of h allows a designer to model in advance nozzle geometry impacts on turbine performance, influencing working fluid impingement angle, the curl of its spiral path, and its residence time. Despite these many changes, the extended model agrees with results published by Carey [1] within 6.4%.

The extended model predicts turbine disks with larger wetted area ($\xi \to 0$) correspond to higher power output. This result, which agrees with the Carey [1] analysis, is intuitive because these disks present more surface area for momentum exchange with the working fluid and the fluid is in contact with the disk over a longer travel path before exiting the turbine.

The extended Tesla turbine model is differentiated with respect to ξ or Re_m^* to evaluate maximum power sensitivity to variable experimental design parameters. This capability of the extended model is particularly important for experimental Tesla turbine design where the goal is not necessarily just maximization of turbine output shaft power. Two important results are indicated from the efficiency (dimensionless power) derivatives. First, turbine power *sensitivity increases* as the wetted disks area decreases. By contrast, *power decreases* as the wetted disk area decreases, indicating an engineering design trade-off between power output and power output sensitivity. Second, for $\xi \leq 0.6$ Tesla turbine power output is uniformly sensitive to working fluid Reynolds number since the power derivative is nearly flat over the whole laminar operating range. Thus, for a given working fluid mass flow rate in the laminar range, Tesla turbine power output will change by a fraction of an order of magnitude while large variation in working fluid properties modulate Reynolds number by more than three orders of magnitude.

Nomenclature

A = area
b = gap distance between disks
c = sonic velocity
h = nozzle parameter—height
$\dot{m}$ = mass flow rate
$\dot{m}_c$ = mass flow rate per channel between disks
n = number of disks
$\hat{n}$ = normal vector
$r, \bar{r}$ = disk radius (scaler and vector forms)
Re_m = Reynolds number based on mass flow rate
Re_m^* = modified Reynolds number based on mass flow rate
r_i = disk radius at turbine inner diameter
r_0 = disk radius at turbine outer diameter
t = disk thickness
U_i = rotor surface tangential velocity at $r = r_i$
U_0 = rotor surface tangential velocity at $r = r_0$
$\bar{V}$ = velocity vector
$\dot{W}$ = turbine shaft power
$\widehat{W}$ = local dimensionless tangential velocity difference
$\widehat{W}_i$ = dimensionless tangential velocity difference at $r = r_i$
$\widehat{W}_0$ = dimensionless tangential velocity difference at $r = r_0$

$\Gamma, \bar{\Gamma}$ = torque (scaler and vector forms)
η = turbine efficiency
μ = viscosity
$\nu_{k,i}, \bar{\nu}_{k,i}$ = k-direction (radial) velocity at the disk inner radius (scaler and vector forms)
$\nu_{k,o}, \bar{\nu}_{k,o}$ = k-direction (radial) velocity at the disk outer radius (scaler and vector forms)
$\nu_{\theta,channel}$ = θ-direction (tangential) velocity entering the channels between disks
$\nu_{\theta,i}, \bar{\nu}_{\theta,i}$ = θ-direction (tangential) velocity at the disk inner radius (scaler and vector forms)
$\nu_{\theta,o}, \bar{\nu}_{\theta,o}$ = θ-direction (tangential) velocity at the disk outer radius (scaler and vector forms)
ξ = dimensionless radial coordinate, $\xi = r/r_0$
ξ_i = dimensionless radial coordinate at disk inner radius, $\xi_i = r_i/r_0$
ρ = density
ω = angular velocity (rad/s)

References

[1] Carey, V. P., 2010, "Assessment of Tesla Turbine Performance for Small Scale Solar Rankine Combined Heat and Power Systems," ASME J. Eng. Gas Turbines Power, **132**(12), p. 122301.
[2] Carey, V. P., 2009, "Assessment of Tesla Turbine Performance for Small Scale Solar Rankine Combined Heat and Power Systems," ASME Paper No. IMECE2009-10814.
[3] Krishnan, V. G., Romanin, V., Carey, V. P., and Maharbiz, M. M., 2013, "Design and Scaling of Microscale Tesla Turbines," J. Micromech. Microeng., **23**(12), p. 125001.
[4] Tesla, N., 1913, "Turbine," U.S. Patent No. 1,061,206.
[5] Tahil, W., 1998, "Theoretical Analysis of a Disk Turbine," Tesla Engine Builder's Association (TEBA) News, Milwaukee, WI, pp. 18–19.
[6] Tahil, W., 1999, "Theoretical Analysis of a Disk Turbine (2)," Tesla Engine Builder's Assoc. (TEBA) News, Milwaukee, WI, pp. 17–18.
[7] Boyd, K. E., and Rice, W., 1968, "Laminar Inward Flow of an Incompressible Fluid Between Rotating Disks, With Full Peripheral Admission," ASME J. Appl. Mech., **35**(2), pp. 229–237.
[8] Rice, W., 1965, "An Analytical and Experimental Investigation of Multiple-Disk Turbines," ASME J. Eng. Power, **87**(1), pp. 29–35.
[9] Matsch, L., and Rice, W., 1968, "An Asymptotic Solution for Laminar Flow of an Incompressible Fluid Between Rotating Disks," ASME J. Appl. Mech., **35**(1), pp. 155–159.
[10] Lawn, M. L., and Rice, W., 1974, "Calculated Design Data for the Multiple-Disk Turbine Using Incompressible Fluid," ASME J. Fluids Eng., **96**(3), pp. 252–258.
[11] Truman, C. R., Rice, W., and Jankowski, D. F., 1978, "Laminar Throughflow of Varying-Quality Steam Between Corotating Disks," ASME J. Fluids Eng., **100**(2), pp. 194–200.
[12] Hoya, G. P., and Guha, A., 2009, "Design of a Test Rig and Study of the Performance and Efficiency of a Tesla Disc Turbine," Proc. Inst. Mech. Eng., Part A, **223**(A4), pp. 451–465.
[13] Guha, A., and Sengupta, S., 2014, "Similitude and Scaling Laws for the Rotating Flow Between Concentric Discs," Proc. Inst. Mech. Eng., Part A, **228**(4), pp. 429–439.
[14] Deng, Q., Qi, W., and Feng, Z., 2013, "Improvement of a Theoretical Analysis Method for Tesla Turbines," ASME Paper No. GT2013-95425.
[15] Qi, W., Deng, Q., Feng, Z., and Yuan, Q., 2016, "Influence of Disc Spacing Distance on the Aerodynamic Performance and Flow Field of Tesla Turbines," ASME Paper No. GT2016-57971.
[16] Guha, A., and Sengupta, S., 2014, "The Fluid Dynamics of Work Transfer in the Non-Uniform Viscous Rotating Flow Within a Tesla Disc Turbomachine," Phys. Fluids, **26**(3), p. 033601.
[17] Yang, Z., Weiss, H. L., and Traum, M. J., 2013, "Gas Turbine Dynamic Dynamometry: A New Energy Engineering Laboratory Module," American Society for Engineering Education (ASEE) North Midwest Section Conference, Fargo, ND, Oct. 17–18, pp. 1–14.
[18] Usman, M., Khan, S., Ali, E., Maqsood, M. I., and Nawaz, H., 2013, "Modern Improved and Effective Design of Boundary Layer Turbine for Robust Control and Efficient Production of Green Energy," J. Phys.: Conf. Ser., **439**(1), p. 012043.
[19] Rice, W., 1991, "Tesla Turbomachinery," Fourth International Tesla Symposium, Serbian Academy of Sciences and Arts, Belgrade, Yugoslavia, Sept. 23–25, pp. 1–12.
[20] Gupta, H. E., and Kodali, S. P., 2013, "Design and Operation of Tesla Turbo Machine—A State of the Art Review," Int. J. Adv. Transp. Phenom., **2**(1), pp. 7–14.
[21] Vidhi, R., Kuravi, S., Goswami, D. Y., Stefanakos, E., and Sabau, A. S., 2013, "Organic Fluids in a Supercritical Rankine Cycle for Low Temperature Power Generation," ASME J. Energy Resour. Technol., **135**(4), p. 042002.
[22] Wong, K. V., and Tan, N., 2015, "Feasibility of Using More Geothermal Energy to Generate Electricity," ASME J. Energy Resour. Technol., **137**(4), p. 041201.
[23] Güell, B. M., Sandquist, J., and Sørum, L., 2012, "Gasification of Biomass to Second Generation Biofuels: A Review," ASME J. Energy Resour. Technol., **135**(1), p. 014001.
[24] Romanin, V. D., Krishnan, V. G., Carey, V. P., and Maharbiz, M. M., 2012, "Experimental and Analytical Study of Sub-Watt Scale Tesla Turbine Performance," ASME Paper No. IMECE2012-89675.
[25] Pandey, R. J., Pudasaini, S., Dhakal, S., Uprety, R. B., and Neopane, H. P., 2014, "Design and Computational Analysis of 1 kW Tesla Turbine," Int. J. Sci. Res. Publ., **4**(11), pp. 314–318.
[26] Hasan, A., and Benzamia, A., 2014, "Investigating the Impact of Air Temperature on the Performance of a Tesla Turbine Using CFD Modeling," Int. J. Eng. Innovation Res., **3**(6), pp. 794–802.
[27] Lampart, P., and Jędrzejewski, L., 2011, "Investigation of Aerodynamics of Tesla Bladeless Microturbines," J. Theor. Appl. Mech., **49**(2), pp. 477–499.
[28] Alrabie, M. S., Altamimi, F. N., Altarrgemy, M. H., Hadi, F., Akbar, M. K., and Traum, M. J., 2017, "Method to Design a Hydro Tesla Turbine for Sensitivity to Varying Laminar Reynolds Number Modulated by Changing Working Fluid Viscosity," ASME Paper No. ES2017-3442.
[29] Choon, T. W., Rahman, A. A., Jer, F. S., and Aik, L. E., 2011, "Optimization of Tesla Turbine Using Computational Fluid Dynamics Approach," IEEE Symposium on Industrial Electronics and Applications (ISIEA), Langkawi, Malaysia, Sept. 25–28, pp. 477–480.
[30] Barbarelli, S., Florio, G., and Scornaienchi, N. M., 2005, "Performance Analysis of a Low-Power Tangential Flow Turbine With Rotary Channel," ASME J. Energy Resour. Technol., **127**(4), pp. 272–279.
[31] Derakhshan, S., and Kasaeian, N., 2014, "Optimization, Numerical, and Experimental Study of a Propeller Pump as Turbine," ASME J. Energy Resour. Technol., **136**(1), p. 012005.
[32] Ho-Yan, B. P., 2011, "Tesla Turbine for Pico Hydro Applications," Guelph Eng. J., **4**, pp. 1–8.
[33] White, F. M., 2011, *Fluid Mechanics*, 7th ed., McGraw-Hill, New York, p. 382.
[34] Yang, Z., Weiss, H. L., and Traum, M. J., 2013, "Dynamic Dynamometry to Characterize Disk Turbines for Space-Based Power," 23rd Annual Wisconsin Space Conference (WSC), Milwaukee, WI, Aug. 15–16, pp. 1–8.
[35] Emran, T. A., 2011, "Tesla Turbine Torque Modeling for Construction of a Dynamometer and Turbine," Master's thesis, University of North Texas, Denton, TX.
[36] Papamoschou, D., 1997, "Mach Wave Elimination in Supersonic Jets," AIAA J., **35**(10), pp. 1604–1611.
[37] Liu, S., Yin, H., Xiong, Y., and Xiao, X., 2016, "A Comparative Analysis of Single Nozzle and Multiple Nozzles Arrangements for Syngas Combustion in Heavy Duty Gas Turbine," ASME J. Energy Resour. Technol., **139**(2), p. 022004.
[38] Beans, E. W., 1961, "Performance Characteristics of a Friction Disk Turbine," Doctoral dissertation, Pennsylvania State University, State College, PA.
[39] Emran, T. A., Alexander, R. C., Stallings, C. T., DeMay, M. A., and Traum, M. J., 2010, "Method to Accurately Estimate Tesla Turbine Stall Torque for Dynamometer or Generator Load Selection," ASME Early Career Technical Conference (ECTC), Atlanta, GA, Oct. 1–2.
[40] Klein, S. A., and Alvarado, F. L., 2002, "Engineering Equation Solver," F-Chart Software, Madison, WI, accessed Sept. 29, 2017, http://www.fchart.com/ees/
[41] Haar, L., Gallagher, J. S., and Kell, G. S., 1984, *NBS/NRC Steam Tables*, Hemisphere Publishing, New York.
[42] Zimmerle, D., and Cirincione, N., 2011, "Analysis of Performance of Direct Dry Cooling for Organic Rankine Cycle Systems," ASME Paper No. ES2011-54202.
[43] Giacomel, J. A., 1987, "Power Translation Device," U.S. Patent No. 4,655,679.
[44] Fréchette, L. G., Lee, C., Arslan, A., and Liu, Y. C., 2003, "Design of a Micro-fabricated Rankine Cycle Steam Turbine for Power Generation," ASME Paper No. IMECE2003-42082.
[45] Epstein, A. H., 2004, "Millimeter-Scale, Micro-Electro-Mechanical Systems Gas Turbine Engines," ASME J. Eng. Gas Turbines Power, **126**(2), pp. 205–226.
[46] Lee, C., and Fréchette, L. G., 2011, "A Silicon Microturbopump for a Rankine-Cycle Power Generation Microsystem—Part I: Component and System Design," J. Microelectromech. Syst., **20**(1), pp. 312–325.
[47] McKeathen, J. E., Reidy, R. F., Boetcher, S. K. S., and Traum, M. J., 2009, "A Cryogenic Rankine Cycle for Space Power Generation," AIAA Paper No. 2009-4247.